SSRG International Journal of Applied Physics
ISSN: 2350-0301/ https://doi.org/10.14445/23500301/IJAP-V13I3P103

Volume 13 Issue 3, 23-35, Sep-Dec 2026
© 2026 Seventh Sense Research Group®

Original Article

Analytical Study of Cosmic Expansion in a Parameterized Dark Energy Model

Doni Nurdiansyah

Indonesia Scientific Society, West Java, Indonesia.

Corresponding Author : doninurdians86@gmail.com

Received: 06 September 2026 Revised: 09 October 2026 Accepted: 28 October 2026 Published: 13 November 2026

Abstract *- The Chevallier–Polarski–Linder (CPL) equation of state, $w(a) = w_0 + w_a(1 - a)$, is the form through which DESI DR2 Baryon Acoustic Oscillation (BAO) data, combined with Cosmic Microwave Background (CMB) and Type Ia supernova (SN Ia) samples, express a preference for evolving dark energy. This study analyses the late-time expansion of a flat universe containing radiation, matter and CPL dark energy, and separates established relations from new results. The dark energy density, Hubble function, deceleration parameter, Om diagnostic and statefinder pair follow from standard relations and are collected only as a common basis. Three contributions go further. First, a pivot-based perturbative solution for the deceleration–acceleration transition redshift z_t is derived; at second order it reproduces the exact root within 0.008 over $-1 \le w_0 \le -0.6$ and $-1.5 \le w_a \le 0$, whereas the conventional first-order expansion about wCDM is in error by up to 0.29 at the DESI-like benchmarks. The solution shows that the earlier onset of acceleration is driven by the slope w_a, while the equation of state at the transition stays close to -1.09 for every benchmark. Second, the acoustic angular scale θ_* is evaluated: the sound horizon is unchanged to better than one part in 10^9, yet the comoving distance to last scattering shifts by up to 0.43%, so θ_* is preserved only if H_0 decreases to 66.5–68.0 km s^{-1} Mpc^{-1} at fixed $\Omega_m h^2$. Third, the closed-form jerk gives the condition $w_a > -3w_0(1 + w_0)$ for $r_0 > 1$, which DESI-like parameters violate; this accounts for the gap between CPL values of r_0 (from -0.82 to -0.06) and cosmographic reports of $j_0 > 1$. For illustrative benchmarks, the dark energy density peaks 7–19% above its present value at $z_c \approx 0.35$–0.44, and z_t lies between 0.74 and 0.78 once Ω_{m0} and H_0 take the values fitted jointly with (w_0, w_a). Future re-deceleration is identified as a property of the linear form, not as a forecast.*

Keywords *- CPL parameterization, Dark energy, DESI, Deceleration parameter, Phantom crossing, Statefinder diagnostic, Transition redshift.*

1. Introduction

Type I a supernovae first showed that the expansion of the Universe is accelerating [1, 2]. CMB anisotropies, BAO and galaxy clustering have since confirmed the result [3]. In the standard ΛCDM model, the acceleration is produced by a cosmological constant with $w = -1$. The model fits most data well, but the observed value of the vacuum energy is hard to reconcile with field-theory estimates, and the near equality of the matter and dark energy densities today looks accidental [4, 5]. These problems keep dynamical alternatives on the table: quintessence, phantom and k-essence fields, interacting dark sectors and modified gravity [5, 6].

No microphysical model is preferred by theory, so observational work usually fits a phenomenological form for $w(z)$. The most widely used is the CPL form [7, 8], $w(a) = w_0 + w_a(1 - a)$. It stays finite at high redshift, contains ΛCDM at $(w_0, w_a) = (-1,0)$, and tracks the late-time behaviour of many scalar-field models [8, 9]. Alternatives such as the Jassal–Bagla–Padmanabhan and Barboza–Alcaniz forms change the high-redshift behaviour while keeping two parameters [10, 11]. Because w_0 and w_a are strongly correlated, constraints are often quoted at a pivot scale factor where w is best measured [12].

The Dark Energy Spectroscopic Instrument (DESI) has turned this phenomenology into a central question. DESI DR2 BAO combined with CMB data prefers CPL over ΛCDM at 3.1σ, and the preference rises to 2.8–4.2σ when SN Ia samples are added [13, 14]. The favoured region, $w_0 > -1$ and $w_a < 0$, implies that w crossed -1 at intermediate redshift. Whether that crossing is physical, statistical or an artefact of the two-parameter form is now debated (Section 2).

The literature reviewed in Section 2 leaves three gaps that motivate this work. First, likelihood analyses report posteriors for (w_0, w_a) but seldom show, in closed form, how these parameters propagate into kinematic quantities such as the transition redshift z_t, the jerk r_0 or the epoch and height of the dark energy maximum. Second, the usual analytic estimate of

This is an open access article under the CC BY-NC-ND license (http://creativecommons.org/licenses/by-nc-nd/4.0/)

z_t, a first-order expansion in w_a about wCDM, fails precisely in the DESI region, and no controlled alternative appears to be available. Third, the claim that DESI-like models leave the CMB acoustic scale unchanged is usually argued from the smallness of early dark energy alone, without a direct evaluation of the distance to last scattering. In parallel, cosmographic analyses of the same data disagree about the sign of $j_0 - 1$, and the source of the disagreement has not been traced through the CPL relations.

This study addresses these gaps for a spatially flat universe with radiation, matter and CPL dark energy. Its contributions, and their status relative to existing work, are as follows:

- Established relations (dark energy density, Hubble function, deceleration parameter, Om, statefinders) are collected with their sources and are not claimed as new; Table 3 lists the status of every relation used.
- A pivot-based perturbative solution for z_t is derived (Equations 20–21). Its accuracy is mapped over the (w_0, w_a) plane and compared with the conventional first-order formula (Equation 19, Table 4 and Figure 1).
- The CMB acoustic scale θ_*, the sound horizon and the comoving distance to last scattering are computed for each benchmark, together with the value of H_0 needed to keep θ_* fixed (Table 6).
- The condition $w_a > -3w_0(1 + w_0)$ for $r_0 > 1$ is obtained from the closed-form jerk and used to compare CPL predictions with recent cosmographic measurements (Equation 30 and Table 8).
- All numerical results are reproduced with stated tolerances and checked against independent calculations (Table 2); their sensitivity to Ω_{m0} and H_0 is quantified (Table 7).

Section 2 reviews related studies. Section 3 sets out the framework, the benchmark models and the numerical procedure. Section 4 presents and discusses the results, and Section 5 concludes. Units with $c = 1$ are used in the equations, and present-day quantities carry the subscript 0.

2. Related Studies

2.1. Evidence for Evolving Dark Energy after DESI DR2

DESI DR2 measured the BAO scale from more than 14 million galaxies and quasars and found the data well described by ΛCDM when taken alone, but in mild tension with CMB-derived parameters within that model [13]. Allowing CPL dark energy relieves the tension. The central values used as benchmarks here come from those combinations: $(w_0, w_a) = (-0.838, -0.62)$ with Pantheon+, $(-0.752, -0.86)$ with DES Y5 and $(-0.667, -1.09)$ with Union3. Lodha et al. [14] extended the analysis to other parameterizations and to non-parametric reconstructions, and found that the preference for dynamics persists, although its strength depends on the form assumed.

Several authors have questioned how robust the signal is. Efstathiou [15] showed that much of the SN-driven preference can be traced to an offset between low- and high-redshift supernovae in the DES Y5 sample. Wang and Mota [16] argued that the BAO, CMB and SN data sets are not fully consistent with one another in the dynamical model, so that their combination may overstate the evidence. Cortês and Liddle [17, 18] pointed out that the inferred phantom crossing and the maximum of the dark energy density fall at the centre of the observed redshift window, a coincidence that calls for explanation; they also argued that the result is sensitive to priors and to the choice of pivot.

2.2. Phantom Crossing: Theory and Statistical Caveats

A single, minimally coupled canonical scalar field cannot cross $w = -1$ without instabilities [19]. Crossing, therefore, requires more structure. Chen et al. [20] built quintessence models with higher powers of the kinetic term, or with a field-dependent dark matter mass, that cross the divide and fit the data better than ΛCDM, but at the cost of moderate tuning and with tight limits from long-range dark matter forces. Efstratiou et al. [21] reconstructed a scalar–tensor theory in which the crossing appears naturally and the inferred H_0 rises to 70.6 ± 1.4 km s^{-1} Mpc^{-1}. Parameterized post-Friedmann methods allow the perturbations of crossing models to be followed consistently [22].

Statistical caveats are equally important. Keeley et al. [23] generated mock data from a non-crossing quintessence model and found that in 3.2% of realisations, a CPL fit improved χ^2 by more than the real data do, so an apparent crossing can arise from noise and from the redshift distribution of the data. Non-parametric reconstructions provide an independent check: a Gaussian-process reconstruction combining DESI with other probes places the crossing at $z \approx 0.46^{+0.24}_{-0.12}$ [24].

2.3. Kinematic and Cosmographic Diagnostics

Kinematic quantities test the expansion history without assuming field equations. The statefinder pair $\{r, s\}$ [25] and the Om diagnostic [26] distinguish dark energy models from ΛCDM through derivatives of $a(t)$ and through $H(z)$ alone. Cosmography expands $d_L(z)$ or $H(z)$ in powers of redshift and relates the coefficients to q_0, the jerk $j_0 \equiv r_0$ and higher derivatives [27].

DESI-era cosmographic results do not agree with one another. Rodrigues et al. [28] found q_0 between -0.42 and -0.51 and j_0 between 1.77 and 2.04, with $j_0 = 1$ excluded at 3.4–5.4σ once SN data are included. Mishra et al. [29] compared Taylor, Padé and Chebyshev expansions of the DR2 data and obtained j_0 from 0.59 to 1.48 depending on the method. Fazzari et al. [30] reported a less negative $q_0 \approx -0.32$ from DESI BAO with a sound-horizon prior. Wang et al. [31], using DESI BAO with CMB information, found

$j(0) < 0$ at more than 1σ and a minimum of $q(z)$ near $z \approx 0.4$, which they interpret as a slowing of the acceleration.

2.4. Research Gap and Position of the Present Study

The studies above approach the problem either through full likelihood fits or through model-independent expansions. The two routes meet only through numerical comparison. Closed-form relations for CPL kinematics are textbook material [6, 8, 25], but they are rarely used to explain why the two routes give different answers, or to quantify which derived features depend on the fixed background parameters. The present work stays at the level of the homogeneous background and adds three things to the existing relations: a controlled analytic approximation for z_t in the regime of large $|w_a|$, a direct evaluation of the CMB acoustic scale for DESI-like benchmarks, and an analytic criterion that links the sign of $r_0 - 1$ to (w_0, w_a).

3. Theoretical Framework and Methods

3.1. Background Dynamics

A spatially flat Friedmann–Lemaître–Robertson–Walker (FLRW) metric is assumed, with scale factor $a(t)$ normalised to $a_0 = 1$ and redshift $1 + z = 1/a$:

$$ds^2 = -dt^2 + a^2(t)[dr^2 + r^2(d\theta^2 + \sin^2\theta\, d\phi^2)] \tag{1}$$

The Universe contains radiation (r), pressureless matter (m, baryons plus cold dark matter) and dark energy (DE). Each component is treated as a perfect fluid with $p_i = w_i\rho_i$, and the Friedmann equations read

$$H^2 = \frac{8\pi G}{3}(\rho_r + \rho_m + \rho_{\mathrm{DE}}), \qquad \frac{\ddot{a}}{a} = -\frac{4\pi G}{3}\sum_i \rho_i\,(1 + 3w_i) \tag{2}$$

The components are assumed to be separately conserved, so that each obeys

$$\dot{\rho}_i + 3H(1 + w_i)\rho_i = 0 \tag{3}$$

This gives $\rho_r \propto a^{-4}$ and $\rho_m \propto a^{-3}$. Density parameters are $\Omega_{i0} = 8\pi G\rho_{i0}/(3H_0^2)$, with $\Omega_{r0} + \Omega_{m0} + \Omega_{\mathrm{DE0}} = 1$.

3.2. The CPL Parameterization

The dark energy equation of state is [7, 8]

$$w(a) = w_0 + w_a(1 - a) = w_0 + w_a\frac{z}{1 + z} \tag{4}$$

Here w_0 is the present value and $w_a = -dw/da$ measures its evolution; w approaches $w_0 + w_a$ as $a \to 0$. The logarithmic derivative, needed for higher-order kinematics, is

$$w' \equiv \frac{dw}{d\ln a} = -w_a\, a \tag{5}$$

The parameter space contains quintessence-like ($w > -1$), phantom-like ($w < -1$) and two crossing ("quintom") regimes. The quadrant $w_0 > -1$, $w_a < 0$ favoured by current data has $w < -1$ in the past and $w > -1$ today.

3.3. Kinematic and Geometric Diagnostics

Beyond $H(z)$, the expansion is characterised by the deceleration parameter q, the jerk r and the second statefinder s [25]:

$$q = -\frac{\ddot{a}\,a}{\dot{a}^2}, \qquad r = \frac{\dddot{a}}{aH^3}, \qquad s = \frac{r - 1}{3\left(q - \frac{1}{2}\right)} \tag{6}$$

For ΛCDM without radiation, $\{r, s\} = \{1,0\}$ at all times. The Om diagnostic [26] equals Ω_{m0} at every redshift if and only if dark energy is a cosmological constant:

$$Om(z) = \frac{E^2(z) - 1}{(1 + z)^3 - 1}, \qquad E(z) \equiv \frac{H(z)}{H_0} \tag{7}$$

The effective equation of state is $w_{\mathrm{eff}} = p_{\mathrm{tot}}/\rho_{\mathrm{tot}} = (2q - 1)/3$. The cosmic age and luminosity distance are

$$t_0 = \frac{1}{H_0}\int_0^1 \frac{da}{a\,E(a)}, \qquad d_L(z) = \frac{1 + z}{H_0}\int_0^z \frac{dz'}{E(z')} \tag{8}$$

3.4. CMB Acoustic Scale

To test whether a benchmark preserves the CMB acoustic scale, the comoving sound horizon at photon decoupling, $r_s(z_*)$, and the comoving distance to that epoch, $D_M(z_*)$, are computed directly:

$$r_s(z_*) = \int_{z_*}^{\infty} \frac{c_s(z)\,dz}{H(z)}, \qquad c_s = \frac{c}{\sqrt{3(1 + R)}}, \quad R = \frac{3\rho_b}{4\rho_\gamma} \tag{9}$$

$$D_M(z_*) = \int_0^{z_*} \frac{c\,dz}{H(z)}, \qquad \theta_* = \frac{r_s(z_*)}{D_M(z_*)} \tag{10}$$

The baryon density $\omega_b \equiv \Omega_b h^2 = 0.02237$ and the decoupling redshift $z_* = 1089.92$ are taken from Planck 2018 [3], and the photon density follows from $T_{\mathrm{CMB}} = 2.7255$ K [32]. Neutrinos are treated as massless, so absolute values of θ_* carry a systematic offset of order 0.02%; the analysis relies on differences between models, for which this offset cancels.

3.5. Benchmark Models and Fixed Parameters

The analytical results are evaluated for ΛCDM and three CPL benchmarks whose. (w_0, w_a) equal the central values

reported by DESI DR2 for BAO combined with CMB and one SN Ia sample [13] (Table 1). These are illustrative benchmark points, not new fits; the 1σ uncertainties of the DESI posteriors are listed so that the spread of the derived quantities can be judged (Figure 2). In the reference setup, all models share $\Omega_{m0} = 0.31$ and $H_0 = 68$ km s^{-1} Mpc^{-1}, chosen close to the Planck 2018 ΛCDM values [3], and $\Omega_{r0} = 9.0 \times 10^{-5}$, which follows from $T_{\rm CMB} = 2.7255$ K [32] with $N_{\rm eff} = 3.046$ and $h = 0.68$; then $\Omega_{\rm DE0} = 1 - \Omega_{m0} - \Omega_{r0}$. Holding these fixed isolates the effect of (w_0, w_a). Because the DESI fits move Ω_{m0} and H_0 together with (w_0, w_a), a second, self-consistent set uses the jointly fitted values listed in Table 1; Section 4.12 compares the two.

Table 1. Benchmark parameters (DESI DR2 central values with 1σ uncertainties [13]). z_c is the phantom-crossing redshift from Equation 22

Model	Data combination	w_0	w_a	Ω_{m0}	H_0 (km s^{-1} Mpc^{-1})	z_c
ΛCDM	Reference	−1	0	0.31	68.00	—
CPL-A	DESI + CMB + Pantheon+	-0.838 ± 0.055	$-0.62^{+0.22}_{-0.19}$	0.3114 ± 0.0057	67.51 ± 0.59	0.354
CPL-B	DESI + CMB + DES Y5	-0.752 ± 0.057	$-0.86^{+0.23}_{-0.20}$	0.3191 ± 0.0056	66.74 ± 0.56	0.405
CPL-C	DESI + CMB + Union3	-0.667 ± 0.088	$-1.09^{+0.31}_{-0.27}$	0.3275 ± 0.0086	65.91 ± 0.84	0.440

3.6. Numerical Procedure and Validation

All calculations were carried out in Python 3.13 with NumPy 2.5 and SciPy 1.18; the script is available from the author on request. Integrals for t_0, d_L, r_s and D_M use adaptive Gauss–Kronrod quadrature (QUADPACK, scipy.integrate.quad) with absolute and relative tolerances 10^{-12} and 10^{-10}. Roots (z_t, $z_{\rm eq}$, a_f and the value of H_0 that restores θ_*) are found with Brent's method at $x_{\rm tol} = 10^{-12}$. Every other quantity uses the closed-form expressions of Section 4.

Four independent checks were made (Table 2). (a) The continuity equation for dark energy was integrated numerically with an eighth-order Runge–Kutta scheme (DOP853, relative tolerance 10^{-12}) from $a = 1$ to $a = 10^{-3}$ and compared with Equation 12. (b) The age was recomputed by integrating dt/da as an ordinary differential equation. (c) The analytic jerk, Equation 27, was compared with $r = q(1 + 2q) + (1 + z)\, dq/dz$ evaluated by central finite differences (step 10^{-5}) on $0 < z \leq 3$. (d) The location and height of the density maximum were found by direct numerical maximisation and compared with Equations 22–23. As an external benchmark, the radiation-free ΛCDM age and transition redshift were compared with their exact analytic values. Finally, for the self-consistent DESI parameters, the code returns $100\theta_* = 1.04089$–1.04097, within 0.02% of the Planck 2018 value 1.04110 ± 0.00031 [3].

Table 2. Numerical validation. Values are maximum absolute (abs.) or relative (rel.) differences between the two methods over the four models.

Check	Comparison	Max. difference
$\rho_{\rm DE}(a)$, $10^{-3} \leq a \leq 1$	Eq. 12 vs ODE	1.0×10^{-12} (rel.)
Age t_0	Quadrature vs ODE	1.0×10^{-12} Gyr
Jerk $r(z)$, $0 < z \leq 3$	Eq. 27 vs finite difference	1.7×10^{-10} (abs.)
$d_L(z = 1)$	Quadrature vs ODE	1.9×10^{-14} (rel.)
a_c and $\rho_{\rm DE}^{\rm max}$	Eqs. 22–23 vs maximisation	1.1×10^{-8}; 2×10^{-16}
ΛCDM t_0 (no radiation)	Analytic 13.736213 Gyr	$< 10^{-12}$ Gyr
ΛCDM z_t (no radiation)	Analytic 0.645025	$< 10^{-12}$
$100\theta_*$, DESI parameters	Planck 2018: 1.04110	0.02% (rel.)

4. Results and Discussion

4.1. Status of the Analytical Relations

Table 3 separates the relations used below into those taken from the literature, those that follow in one or two lines from them, and those derived or evaluated for the first time here, to the best of the author's knowledge. Equations 12–16, 22, 24–28 are standard and serve as a reference set. Equations 16 and 23 are elementary consequences of the CPL definition; they are kept because they are used repeatedly and because Equation 23 gives the height of the density maximum in a compact form. The new material lies in Equations 20–21, Equation 30 and the numerical assessments of Sections 4.11–4.13.

Table 3. Status of the relations used in this study

Equation	Quantity	Status
11–13	$\rho_{\rm DE}(z)$, $E(z)$	Established [7, 8]
14	Low-z expansion of E^2	Standard; restated
15–16	$q(z)$, q_0	Standard; q_0 follows from $w(0)=w_0$
17–19	z_t condition; first order about wCDM	Derived here; validity limited (Sec. 4.5)
20–21	Pivot-based z_t to second order	New in this work
22–23	a_c, $\rho_{\rm DE}^{\rm max}$	Elementary; compact form given
24–25	Asymptotic limits	Standard [33]
26–28	Om limit, $r(z)$, r_0, s_0	General form [25, 26]; CPL case
30	Condition for $r_0 > 1$	New consequence of Eq. 28
—	θ_*, H_0 compensation	New numerical assessment

4.2. Evolution of the Dark Energy Density

Substituting Equation 4 into Equation 3 gives $d\ln\rho_{\rm DE}/d\ln a = -3[1+w_0+w_a(1-a)]$. Integrating from $a=1$,

$$\ln\frac{\rho_{\rm DE}}{\rho_{\rm DE0}} = -3(1+w_0+w_a)\ln a - 3w_a(1-a) \tag{11}$$

so that

$$f(a)\equiv\frac{\rho_{\rm DE}(a)}{\rho_{\rm DE0}} = a^{-3(1+w_0+w_a)}e^{-3w_a(1-a)},$$
$$f(z) = (1+z)^{3(1+w_0+w_a)}\exp\left[-\frac{3w_a z}{1+z}\right] \tag{12}$$

The power-law factor is that of a constant-w fluid with $w = w_0 + w_a$; the exponential carries the late-time approach to w_0.

4.3. The Hubble Function

The first Friedmann equation becomes

$$E^2(z) = \Omega_{r0}(1+z)^4 + \Omega_{m0}(1+z)^3 + \Omega_{\rm DE0}(1+z)^{3(1+w_0+w_a)}\exp\left[-\frac{3w_a z}{1+z}\right] \tag{13}$$

Expanding about $z=0$,

$$E^2(z) \simeq 1 + 3\left[1 + w_0\Omega_{\rm DE0} + \frac{1}{3}\Omega_{r0}\right]z + \mathcal{O}(z^2) \tag{14}$$

The parameter w_a enters only at order z^2. Low-redshift distances, therefore fix w_0 more tightly than w_a, which is the origin of the familiar w_0–w_a degeneracy [13, 18].

4.4. Deceleration Parameter

From the second Friedmann equation, $q = \frac{1}{2}\sum_i \Omega_i(z)(1+3w_i)$, which gives

$$q(z) = \frac{1}{2E^2(z)}\{2\Omega_{r0}(1+z)^4 + \Omega_{m0}(1+z)^3 + \Omega_{\rm DE0}f(z)[1+3w(z)]\} \tag{15}$$

At $z=0$, with $f = E = 1$ and $w = w_0$,

$$q_0 = \frac{1}{2}(1 + \Omega_{r0} + 3w_0\Omega_{\rm DE0}) \tag{16}$$

The absence of w_a in q_0 is not a new result: it follows directly from $w(0)=w_0$, since q_0 depends only on the present densities and pressures. Its practical consequence is still worth stating. A cosmographic fit that constrains only q_0 cannot detect evolution of w; the evolution first enters through the jerk (Section 4.9). With $w_{\rm eff} = (2q-1)/3$ one also has $w_{\rm eff,0} = \Omega_{r0}/3 + w_0\Omega_{\rm DE0}$.

4.5. Transition Redshift: First-Order Expansion about wCDM

The transition redshift is defined by $q(z_t)=0$. Radiation contributes less than 10^{-3} to q for $z<3$ and is neglected in the analytic treatment. Writing $x \equiv 1+z_t$, the condition reads

$$\Omega_{m0} + \Omega_{\rm DE0}\,x^{3(w_0+w_a)}e^{-3w_a(1-x^{-1})} \times [1 + 3w_0 + 3w_a(1-x^{-1})] = 0 \tag{17}$$

This equation has no closed-form solution for $w_a \neq 0$. For $w_a = 0$ (wCDM) it gives

$$x_0 \equiv 1 + z_t^{(0)} = \left[-(1+3w_0)\frac{\Omega_{\rm DE0}}{\Omega_{m0}}\right]^{-1/(3w_0)} \tag{18}$$

which reduces to $x_0 = (2\Omega_\Lambda/\Omega_{m0})^{1/3}$ for ΛCDM. Expanding Equation 17 to first order in w_a about x_0 at fixed w_0 gives

$$1 + z_t \simeq x_0\left(1 - \frac{w_a}{w_0}B_0\right),$$
$$B_0 \equiv \ln x_0 - 1 + \frac{1}{x_0} + \frac{1 - x_0^{-1}}{1 + 3w_0} \quad (19)$$

Equation 19 is accurate to about 0.01 for $|w_a| \lesssim 0.25$–0.3 when $-1 \le w_0 \le -0.7$ (Table 4 and Figure 1a), which covers the mild evolution considered before DESI. It fails in the DESI region. At the benchmarks, it overestimates z_t by 0.06, 0.15 and 0.29, and its second-order extension (not shown) diverges further for CPL-C.

The reason is structural: the expansion starts from a wCDM model with $w = w_0$, whereas the transition takes place at $z \approx 0.6$–0.9, where w in the DESI quadrant is already below -1. The zeroth-order term then points in the wrong direction, raising w_0 alone lowers z_t, and the first-order term has to overcompensate. Equation 19 should therefore be used only for $|w_a| \lesssim 0.3$.

4.6. Pivot-Based Solution for the Transition Redshift

A better starting point is a constant-w model whose equation of state equals the CPL value at the transition itself. Rewriting Equation 4 about a pivot scale factor a_p, in the spirit of pivot parameterizations [12], gives $w(a) = w_p + w_a(a_p - a)$ with $w_p \equiv w(a_p)$.

Equation 17 is then expanded in w_a at fixed (w_p, a_p), and only afterwards is the pivot placed at the zeroth-order transition, $a_p = 1/x_p$. This choice cancels the large terms of Equation 19 and leaves corrections controlled by $x_p - \ln x_p - 1$, which is small near the transition. The zeroth-order solution satisfies.

$$x_p = \left[-(1 + 3w_p)\frac{\Omega_{\mathrm{DE0}}}{\Omega_{m0}}\right]^{-1/(3w_p)},$$
$$w_p = w_0 + w_a(1 - x_p^{-1}) \quad (20)$$

and the result to second order in w_a is

$$1 + z_t \simeq x_p + \frac{w_a}{w_p}D + \frac{w_a^2 D\left[(1 + 3w_p)D - 2\right]}{2w_p^2 x_p(1 + 3w_p)},$$
$$D \equiv x_p - \ln x_p - 1 \quad (21)$$

Equation 20 is a one-dimensional fixed-point problem. Starting from the wCDM value x_0, the iteration $x_p \leftarrow x_p\left(w_0 + w_a(1 - x_p^{-1})\right)$ converges to 10^{-10} in six to eight steps at the benchmarks.

A single step already gives an explicit formula, with errors of 0.0005, 0.004 and 0.023 for CPL-A, B and C. Equations 20–21 were derived symbolically and checked against the exact root on an 81×121 grid in the (w_0, w_a) plane (Figure 1b).

Result 1. Over $-1 \le w_0 \le -0.6$ and $-1.5 \le w_a \le 0$ the pivot solution has a maximum error of 0.0077 and a median error of 0.0006 in z_t; for $-1 \le w_0 \le -0.7$ the error stays below 0.01 for $-2 \le w_a \lesssim 0.4$. The first-order expansion about wCDM has a median error of 0.087 over the same region. The accuracy is lost only for large positive w_a, where w becomes strongly phantom today, and the fixed point moves away from the transition.

The pivot solution also explains the physics of the shift. For all three benchmarks, the self-consistent pivot gives $w_p = -1.080$, -1.088 and -1.093, and the zeroth-order term $x_p - 1 = 0.642$, 0.641, 0.641, almost the ΛCDM value of 0.645. The equation of state at the transition is therefore nearly the same in all three models, and the earlier onset of acceleration (Table 4) comes from the first- and second-order terms, that is, from the slope w_a.

In words, DESI-like dark energy begins to accelerate the expansion earlier because it was more strongly repulsive just before the transition, not because its equation of state at the transition is very different from -1.

Table 4. Transition redshift from the wCDM value (Eq. 18), the first-order formula (Eq. 19), the pivot solution at first and second order (Eq. 21) and the exact root, for $\Omega_{m0} = 0.31$

w_0	w_a	wCDM	Eq. 19	Pivot, 1st	Pivot, 2nd	Exact
−1.000	+0.30	0.645	0.600	0.585	0.592	0.591
−1.000	−0.30	0.645	0.690	0.677	0.681	0.680
−0.900	−0.30	0.637	0.705	0.688	0.693	0.692
−0.838	−0.62	0.621	0.805	0.726	0.741	0.741
−0.752	−0.86	0.577	0.941	0.756	0.785	0.787
−0.667	−1.09	0.492	1.124	0.786	0.831	0.834

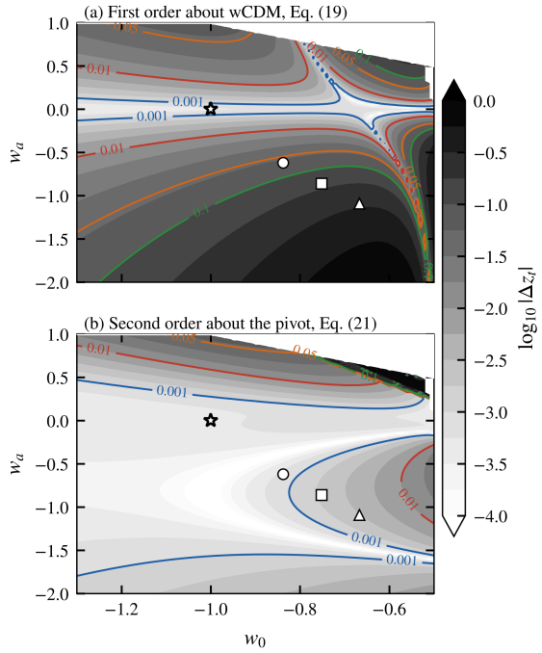


Fig. 1 Absolute error $|\Delta z_t|$ of (a) the first-order expansion about wCDM, Equation 19, and (b) the second-order pivot solution, Equation 21, relative to the exact root of $q = 0$. Contours mark 0.001, 0.01, 0.05 and 0.1. Circle, square and triangle: CPL-A, B, C; star: ΛCDM. The blank region has $w_0 + w_a \geq 0$

4.7. Phantom-Divide Crossing and the Dark Energy Maximum

The equation of state crosses $w = -1$ at

$$a_c = 1 + \frac{1 + w_0}{w_a}, \qquad z_c = -\frac{1 + w_0}{1 + w_0 + w_a} \tag{22}$$

The crossing lies in the past ($0 < a_c < 1$) when $1 + w_0$ and w_a have opposite signs and $|1 + w_0| < |w_a|$. Because $d\ln\rho_{\rm DE}/d\ln a = -3(1 + w)$, the density is stationary at a_c: a maximum for $w_a < 0$ and a minimum for $w_a > 0$. Using $1 + w_0 + w_a = w_a a_c$, Equation 12 evaluated at a_c becomes

$$\frac{\rho_{\rm DE}^{\rm max}}{\rho_{\rm DE0}} = a_c^{-3w_a a_c} \exp[-3w_a(1 - a_c)] \tag{23}$$

Both expressions are elementary consequences of Equations 4 and 12; their use here is quantitative. Figure 2 maps z_c and $\rho_{\rm DE}^{\rm max}/\rho_{\rm DE0}$ over the (w_0, w_a) plane together with the DESI 1σ ranges. Contours of z_c fan out from $(w_0, w_a) = (-1,0)$ and run roughly along the DESI degeneracy direction, so the crossing redshift is better determined than either parameter separately. Over the rectangular 1σ ranges of Table 1, z_c spans 0.15–1.2 and the density excess 2–53%; because the true posteriors are elongated along the degeneracy, nearly parallel to the z_c contours, the actual spread of z_c is smaller. The height of the maximum grows quickly as w_0 moves away from -1 at fixed w_a, which makes it a sensitive but poorly constrained quantity.

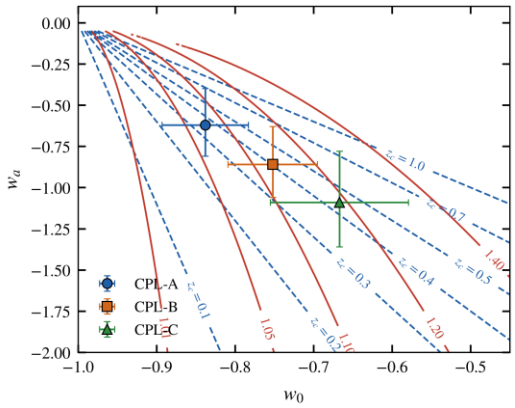


Fig. 2 Contours of the phantom-crossing redshift z_c (dashed, Equation 22) and of the density maximum $\rho_{\rm DE}^{\rm max}/\rho_{\rm DE0}$ (solid, Equation 23) in the (w_0, w_a) plane. Points with error bars are the benchmarks with their DESI DR2 1σ marginal uncertainties

4.8. Asymptotic Regimes

Early times ($a \to 0$). The ratio of dark energy to matter behaves as

$$\frac{\rho_{\rm DE}}{\rho_m} \overset{a\to 0}{\to} \frac{\Omega_{\rm DE0}}{\Omega_{m0}}\, e^{-3w_a}\, a^{-3(w_0+w_a)} \tag{24}$$

A matter-dominated era, therefore requires $w_0 + w_a < 0$, a condition imposed as a prior in observational analyses [13]. For the benchmarks $w_0 + w_a$ lies between -1.46 and -1.76, and $\Omega_{\rm DE}$ at $z = 1100$ is below 10^{-12} (Table 5).

Future ($a \to \infty$). For $w_a < 0$, $w(a) = w_0 + |w_a|(a - 1)$ grows without bound and

$$f(a) \propto a^{-3(1+w_0+w_a)}\, e^{-3|w_a|a} \overset{a\to\infty}{\to} 0 \tag{25}$$

Matter then dominates again, $q \to \frac{1}{2}$, and acceleration ends at a finite scale factor $a_f > 1$. For $w_a > 0$ the density grows as $e^{3w_a a}$ and the model ends in a finite-time singularity similar to a big rip [33]. Both outcomes come from extrapolating a form linear in a far beyond the data; they are mathematical properties of the parameterization and are not presented as predictions (Section 4.15).

4.9. Om and Statefinder Diagnostics

Combining Equations 7 and 14 and neglecting radiation,

$$\lim_{z\to 0} Om(z) = \Omega_{m0} + \Omega_{\rm DE0}(1 + w_0) \tag{26}$$

So Om exceeds Ω_{m0} at low redshift whenever $w_0 > -1$, independently of w_a. Differentiating q and neglecting radiation gives the jerk.

$$r(z) = 1 + \frac{9}{2}\Omega_{\rm DE}(z)\, w(z)[1 + w(z)] + \frac{3}{2}\Omega_{\rm DE}(z)\, w_a\, a \tag{27}$$

which is the general statefinder expression [25] with Equation 5 inserted. Its present value and the second statefinder are

$$r_0 = 1 + \frac{9}{2}\Omega_{\mathrm{DE0}} w_0(1 + w_0) + \frac{3}{2}\Omega_{\mathrm{DE0}} w_a, \qquad s_0 = \frac{r_0 - 1}{3\left(q_0 - \frac{1}{2}\right)} \tag{28}$$

In the luminosity-distance expansion [27]

$$H_0 d_L = z + \frac{1}{2}(1 - q_0)z^2 - \frac{1}{6}(1 - q_0 - 3q_0^2 + r_0)z^3 + \cdots \tag{29}$$

w_a first appears at third order, through r_0, with coefficient $\frac{3}{2}\Omega_{\mathrm{DE0}} \approx 1.04$. Setting $r_0 > 1$ in Equation 28 and dividing by $\frac{3}{2}\Omega_{\mathrm{DE0}} > 0$ gives

$$r_0 > 1 \Leftrightarrow w_a > -3w_0(1 + w_0) \tag{30}$$

Result 2. For $w_0 > -1$ the right-hand side of Equation 30 is positive (0.41, 0.56 and 0.67 for the benchmarks), whereas DESI finds $w_a < 0$. Every model in the DESI quadrant, therefore has $r_0 < 1$, and the benchmarks give $r_0 = -0.06$, -0.47 and -0.82. Figure 3 shows that $r(z)$ rises through unity at $z \approx 0.76$–0.85 and exceeds 1 by 9–14% near $z \approx 1.4$, while $Om(z)$ falls from 0.42–0.54 at $z \to 0$ to slightly below Ω_{m0} beyond $z \approx 0.9$–1.2. The negative slope dOm/dz at low redshift is the signature of quintessence-like behaviour today [26].

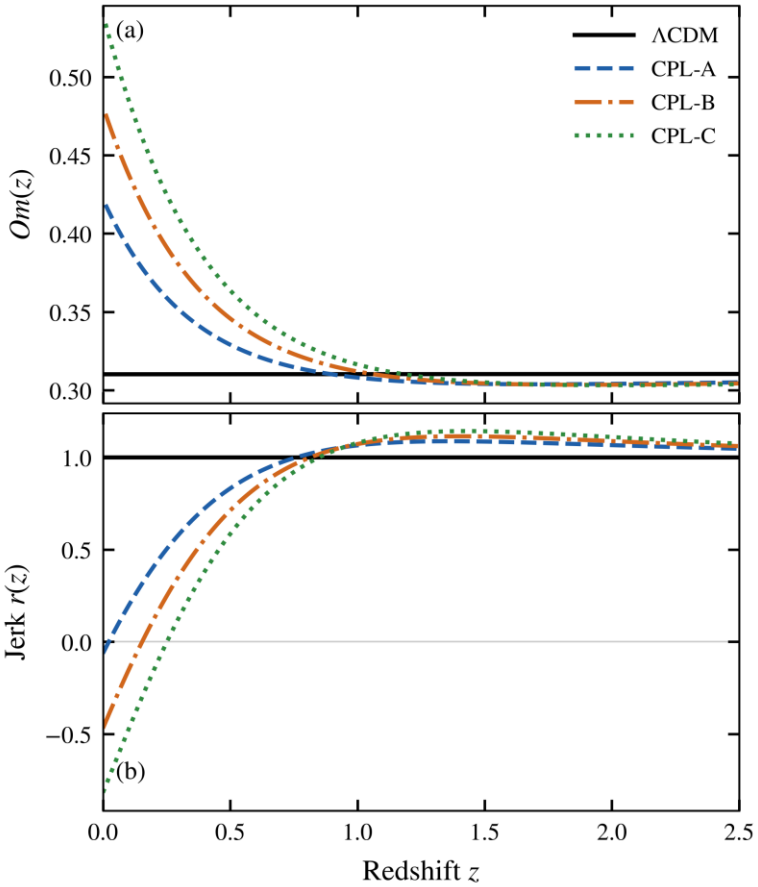


Fig. 3 (a) $Om(z)$ diagnostic, Equation 7, and (b) jerk parameter $r(z)$, Equation 27, for the four benchmark models. ΛCDM has $Om = \Omega_{m0}$ and $r = 1$ at all redshifts

4.10. Expansion History of the Benchmark Models

Table 5 lists the derived quantities in the reference setup. All three CPL models reach a dark energy maximum 7–19% above today's value at $z_c = 0.35$–0.44 (Figure 5), accelerate earlier than ΛCDM ($z_t = 0.74 - 0.83$ against 0.64) and accelerate less strongly today (q_0 between -0.37 and -0.19). Figure 4 shows that the CPL curves cross $q = 0$ earlier but lie above ΛCDM for $z \lesssim 0.3$. For CPL-B and CPL-C, $q(z)$ has a minimum at $z = 0.11$ and $z = 0.21$; this is the kinematic imprint of the density maximum, and it means that acceleration has been weakening since then. CPL-A has no such minimum for $z > 0$. The differences in $H(z)$ and in the distance modulus are small, below 4% and 0.07 mag, which is why percent-level BAO precision is needed to see them [13].

Table 5. Derived quantities in the reference set-up ($\Omega_{m0} = 0.31$, $H_0 = 68$ km s^{-1} Mpc^{-1}). $\Delta\mu$ is the distance-modulus difference relative to ΛCDM

Quantity (unit)	ΛCDM	CPL-A	CPL-B	CPL-C
Deceleration parameter today, q_0	−0.535	−0.367	−0.278	−0.190
Effective EoS today, $w_{\mathrm{eff},0}$	−0.690	−0.578	−0.519	−0.460
Transition redshift, z_t ($q = 0$)	0.644	0.741	0.787	0.834
Matter–DE equality, z_{eq}	0.306	0.336	0.358	0.381
Phantom crossing, z_c	—	0.354	0.405	0.440
DE maximum, $\rho_{\mathrm{DE}}^{\max}/\rho_{\mathrm{DE0}}$	1	1.072	1.127	1.187
Age, t_0 (Gyr)	13.73	13.68	13.61	13.54
Jerk today, r_0	1.000	−0.063	−0.469	−0.818
Statefinder today, s_0	0	0.409	0.629	0.878
$Om(z = 0.5)$	0.310	0.329	0.346	0.364
$\Delta\mu(z = 0.5)$ (mag)	0	−0.030	−0.050	−0.071
$\Delta\mu(z = 1.0)$ (mag)	0	−0.022	−0.040	−0.060
$H/H_{\Lambda\mathrm{CDM}}$ at $z = 0.5$	1	1.013	1.024	1.036
Ω_{DE} at $z = 1100$	1.3×10^{-9}	5.4×10^{-13}	4.3×10^{-14}	4.1×10^{-15}
Re-deceleration scale factor, a_f	—	1.73	1.39	1.21
Time from today to a_f (Gyr)	—	9.6	5.4	2.9

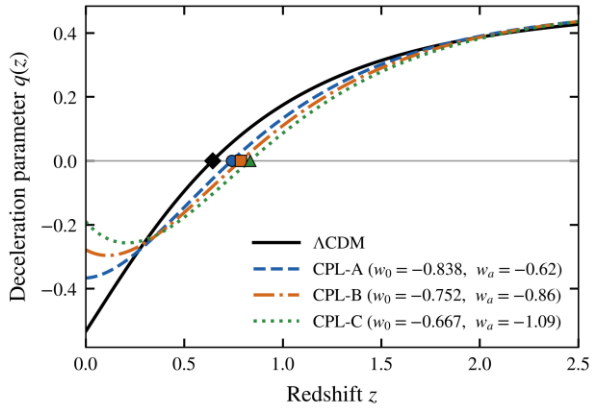


Fig. 4 Deceleration parameter $q(z)$, Equation 15, for the four benchmark models. Markers show the transition redshift z_t where $q = 0$. The minima of the CPL-B and CPL-C curves at $z = 0.11$ and 0.21 reflect the dark energy density maximum

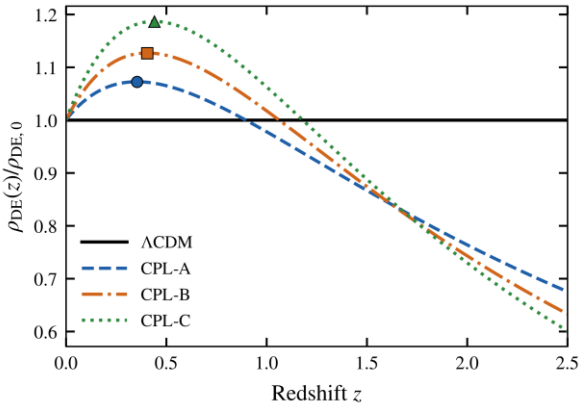


Fig. 5 Normalised dark energy density $\rho_{\mathrm{DE}}(z)/\rho_{\mathrm{DE0}}$ from Equation 12. Markers show the maxima at the phantom-crossing redshift, Equations 22–23

4.11. CMB Acoustic Scale

The original argument that DESI-like models leave the CMB unchanged rests on the smallness of early dark energy. Table 6 tests it directly. The first part of the argument holds: with $\Omega_{\mathrm{DE}} < 10^{-12}$ at decoupling, the sound horizon is the same in all four models to better than one part in 10^9, $r_s = 144.39$ Mpc.

The second part does not follow. The comoving distance $D_M(z_*)$ is an integral over the whole expansion history, and late-time dark energy changes it. At fixed H_0 and Ω_{m0} the shift is negligible for CPL-A (3×10^{-6}), because the density excess before z_c and the deficit after it nearly cancel in the integral.

For CPL-B and CPL-C, D_M falls by 0.20% and 0.43%, and θ_* rises by the same amount. Planck measures $100\theta_*$ to 0.03% [3], so these shifts correspond to about 7σ and 14σ.

Result 3. The acoustic scale is preserved only if other parameters move. Keeping $\omega_m = \Omega_{m0}h^2$ and ω_b fixed, θ_* is restored for $H_0 = 67.28$ and 66.52 km s^{-1} Mpc^{-1} (CPL-B and C), with $\Omega_{m0} = 0.317$ and 0.324.

These values follow the same trend as the DESI joint fits in Table 1, which shows that the geometric degeneracy with the CMB, rather than any effect at recombination, drives the lower H_0 of DESI-preferred CPL models.

The earlier statement that the benchmarks "leave the CMB acoustic scale essentially unchanged" is therefore valid only for the sound horizon, and is corrected here.

Table 6. CMB acoustic quantities at $z_* = 1089.92$. Columns 2–5 use the reference setup; the last three rows give the parameters that restore the ΛCDM value of θ_* at fixed ω_m and ω_b

Quantity (unit)	ΛCDM	CPL-A	CPL-B	CPL-C
Sound horizon $r_s(z_*)$ (Mpc)	144.39	144.39	144.39	144.39
$D_M(z_*)$ (Mpc)	13831.3	13831.3	13803.1	13772.4
$100\,\theta_*$	1.04392	1.04392	1.04605	1.04838
$\Delta\theta_*/\theta_*$ (%)	0	−0.0003	+0.204	+0.427
H_0 restoring θ_* (km s^{-1} Mpc^{-1})	68.00	68.00	67.28	66.52
Ω_{m0} restoring θ_*	0.310	0.310	0.317	0.324
z_t with restored H_0, Ω_{m0}	0.644	0.742	0.767	0.792

4.12. Sensitivity to Ω_{m0} and H_0

The reference setup fixes Ω_{m0} and H_0 to isolate (w_0, w_a), but this choice affects some conclusions. Table 7 repeats the calculation with the DESI joint values. Quantities that depend only on (w_0, w_a), namely z_c and $\rho_{\rm DE}^{\rm max}/\rho_{\rm DE0}$, do not change. The transition redshift moves down to 0.737–0.781, so the spread between benchmarks shrinks from 0.09 to 0.04. A change of ± 0.01 in Ω_{m0} alone shifts z_t by about ∓ 0.03, as large as the difference between neighbouring benchmarks. The age changes most: with the DESI values, all three models give $t_0 = 13.76$ Gyr, so the reduction of 0.05–0.19 Gyr relative to ΛCDM in Table 5 is a consequence of fixing H_0 and should not be read as a property of evolving dark energy. The jerk remains strongly negative for CPL-B and C.

Table 7. Sensitivity of derived quantities to the background parameters. "Fixed": $\Omega_{m0} = 0.31$, $H_0 = 68$; "DESI": joint values of Table 1

Quantity	A fixed	A DESI	B fixed	B DESI	C fixed	C DESI
z_t	0.741	0.737	0.787	0.760	0.834	0.781
z_t, Eq. 21	0.741	0.737	0.785	0.758	0.831	0.777
q_0	−0.367	−0.365	−0.278	−0.268	−0.190	−0.173
$z_{\rm eq}$	0.336	0.333	0.358	0.339	0.381	0.343
t_0 (Gyr)	13.68	13.76	13.61	13.76	13.54	13.76
r_0	−0.063	−0.061	−0.469	−0.450	−0.818	−0.771
$100\,\theta_*$	1.0439	1.0409	1.0461	1.0410	1.0484	1.0409
z_t, $\Omega_{m0} = 0.30$	0.770	—	0.817	—	0.866	—
z_t, $\Omega_{m0} = 0.32$	0.713	—	0.757	—	0.804	—

4.13. Comparison with Previous Studies

Table 8 compares the benchmark predictions with recent independent analyses. Three points stand out.

First, the present-day deceleration parameter. The CPL benchmarks give q_0 between -0.37 and -0.17, less negative than the cosmographic values of -0.40 to -0.51 [28, 29] but in line with $q_0 \approx -0.32$ from DESI BAO with a sound-horizon prior [30]. Fazzari et al. noted that a less negative q_0 is expected for dynamical dark energy; Equation 16 makes the reason explicit, since q_0 rises linearly with w_0 at a rate $\frac{3}{2}\Omega_{\rm DE0}$.

Second, the jerk. Rodrigues et al. [28] found $j_0 \approx 1.8$–2.0, while CPL benchmarks give $r_0 < 0$. Equation 30 shows that no CPL model with $w_0 > -1$ and $w_a < 0$ can have $r_0 > 1$, so the disagreement is structural and not a matter of error bars; Rodrigues et al. likewise noted that $j_0 > 1$ in CPL requires parameter values disfavoured by current fits. The spread of j_0 between 0.59 and 1.48 across expansion methods [29] suggests that the truncation of cosmographic series is part of the problem. The negative $j(0)$ found by Wang et al. [31] from DESI BAO plus CMB is consistent in sign with CPL-B and CPL-C, as is their minimum of $q(z)$, although they place it at $z \approx 0.4$ and the benchmarks at 0.1–0.2.

Third, the crossing redshift. The benchmarks give $z_c = 0.35$–0.44, consistent with the Gaussian-process value of $0.46^{+0.24}_{-0.12}$ [24], and Figure 2 shows that z_c runs along the DESI degeneracy direction. This supports the observation of Cortês and Liddle [17, 18] that the crossing tends to sit where the data are most informative, a feature that may partly reflect the projection of the data onto a two-parameter form [23].

Table 8. Comparison of benchmark predictions with recent independent results

Quantity	This work	Other studies
q_0	−0.37 to −0.19 (fixed); −0.37 to −0.17 (DESI)	−0.42 to −0.51 [28]; −0.40 to −0.49 [29]; −0.32 [30]
$j_0 = r_0$	−0.82 to −0.06	1.77 to 2.04 [28]; 0.59 to 1.48 [29]; $j(0) < 0$ at >1σ [31]
Minimum of $q(z)$	$z = 0.11$, 0.21 (B, C)	$z \approx 0.4$ [31]
z_c $(w = -1)$	0.35 to 0.44	$0.46^{+0.24}_{-0.12}$ [24]; centre of data window [18]
z_t	0.74 to 0.83 (fixed); 0.74 to 0.78 (DESI)	0.64 (ΛCDM, this work); ≈0.7 [29]
H_0 (km s^{-1} Mpc^{-1})	66.5 to 68.0 to keep θ_*	65.9 to 67.5 [13]

4.14. Physical Interpretation of the Phantom Crossing

In the favoured quadrant, the dark energy density grew until $z_c \approx 0.35$–0.44 and has declined since. Before z_c The null energy condition is violated in the dark sector. A minimally coupled canonical field cannot do this [19]. Possible realisations include two-field quintom models, fields with non-canonical kinetic terms or coupling to dark matter [20], and scalar–tensor theories in which the effective w crosses -1 without ghosts [21].

In interacting models, an apparent phantom phase can also appear when the matter density is assumed to scale as a^{-3} while it does not. The background results of this study cannot discriminate among these options; they show only which kinematic signatures any successful model must reproduce, namely $r_0 < 0$, a weakening of acceleration since $z \approx 0.1$–0.2, and a transition at $z_t \approx 0.74$–0.78.

4.15. Limits of the Parameterization and of This Study

The CPL form is a first-order expansion around $a = 1$ and is reliable only over the range probed by data, roughly $0 \leq z \lesssim 2.5$. Three consequences follow. The re-deceleration within 3–10 Gyr for $w_a < 0$ and the finite-time singularity for $w_a > 0$ (Section 4.8) result from extrapolating w to $|w| \to \infty$; they are listed in Table 5 for completeness only and are not forecasts. The condition $w_0 + w_a < 0$ is required for a matter era, but has no physical motivation, and it acts as an implicit prior on large negative w_a. Whether the crossing survives a change of form must be tested with other parameterizations [10, 11] and with non-parametric reconstructions [14, 24].

The study itself is limited to a homogeneous background and to illustrative central values. Linear perturbations, the growth rate $f\sigma_8(z)$ and the stability of crossing models requires a separate treatment, for example, with the parameterized post-Friedmann approach [22].

Massive neutrinos were neglected in the CMB calculation, and the propagation of the full DESI posterior through the derived quantities would require the posterior samples rather than marginal errors. Within these limits, the analytical relations provide fast and checkable values for the quantities most often used to interpret the DESI signal.

5. Conclusion

The late-time expansion of a flat universe with CPL dark energy has been analysed with a clear separation between known relations and new results. The established closed forms for $\rho_{\rm DE}$, $E(z)$, $q(z)$, Om and the statefinders were collected and validated against independent numerical calculations. Beyond them, the study reached three conclusions.

(i) The conventional first-order formula for the transition redshift is accurate only for $|w_a| \lesssim 0.3$ and fails by up to 0.29 at DESI-like parameters. A pivot-based second-order solution, Equations 20–21, reduces the error to below 0.008 over the region favoured by DESI and shows that the earlier onset of acceleration is driven by w_a, with $w \approx -1.09$ at the transition in all benchmarks.

(ii) Negligible early dark energy keeps the sound horizon unchanged, but does not keep θ_* unchanged. For two of the three benchmarks, the acoustic scale shifts by 7–14 times the Planck uncertainty unless H_0 decreases to 66.5–67.3 km s^{-1} Mpc^{-1}, the same trend as in the DESI joint fits.

(iii) The condition $w_a > -3w_0(1 + w_0)$ for $r_0 > 1$ excludes the entire DESI quadrant, which explains why CPL benchmarks give $r_0 < 0$ while some cosmographic analyses report $j_0 > 1$.

For illustrative DESI DR2 benchmarks, the dark energy density peaks 7–19% above its present value at $z_c \approx 0.35$–0.44, and the transition redshift lies between 0.74 and 0.78 when Ω_{m0} and H_0 Take their jointly fitted values. The reduction of the cosmic age and the future return to deceleration depend, respectively, on the fixed background parameters and on the extrapolation of the linear form, and should not be quoted as physical predictions. Extending the pivot method to the growth rate and to other parameterizations is the natural next step.

Conflicts of Interest

The author declares that there is no conflict of interest regarding the publication of this paper.

Funding Statement

This research received no specific grant from any funding agency in the public, commercial, or not-for-profit sectors.

References

[1] Adam G. Riess et al., "Observational Evidence from Supernovae for an Accelerating Universe and a Cosmological Constant," *The Astronomical Journal*, vol. 116, no. 3, pp. 1009-1038, 1998. [CrossRef] [Google Scholar] [Publisher Link]

[2] Saul Perlmutter et al., "Measurements of Ω and Λ from 42 High-Redshift Supernovae," *The Astrophysical Journal*, vol. 517, no. 2, pp. 565-586, 1999. [CrossRef] [Google Scholar] [Publisher Link]

[3] Nabila Aghanim et al., "Planck 2018 Results. VI. Cosmological Parameters," *Astronomy & Astrophysics*, vol. 641, pp. 1-67, 2020. [CrossRef] [Google Scholar] [Publisher Link]

[4] Steven Weinberg, "The Cosmological Constant Problem," *Reviews of Modern Physics*, vol. 61, no. 1, pp. 1-23, 1989. [CrossRef] [Google Scholar] [Publisher Link]

[5] Edmund J. Copeland, Mohammad Sami, and Shinji Tsujikawa, "Dynamics of Dark Energy," *International Journal of Modern Physics D*, vol. 15, no. 11, pp. 1753-1935, 2006. [CrossRef] [Google Scholar] [Publisher Link]

[6] Luca Amendola, and Shinji Tsujikawa, *Dark Energy: Theory and Observations*, Cambridge University Press, 2010. [CrossRef] [Google Scholar] [Publisher Link]

[7] Michel Chevallier, and David Polarski, "Accelerating Universes with Scaling Dark Matter," *International Journal of Modern Physics D*, vol. 10, no. 2, pp. 213-223, 2001. [CrossRef] [Google Scholar] [Publisher Link]

[8] Eric V. Linder, "Exploring the Expansion History of the Universe," *Physical Review Letters*, vol. 90, no. 9, pp. 1-4, 2003. [CrossRef] [Google Scholar] [Publisher Link]

[9] Eric V. Linder, "Paths of Quintessence," *Physical Review D*, vol. 73, no. 6, pp. 1-12, 2006. [CrossRef] [Google Scholar] [Publisher Link]

[10] H.K. Jassal, J.S. Bagla, and T. Padmanabhan, "WMAP Constraints on Low Redshift Evolution of Dark Energy," *Monthly Notices of the Royal Astronomical Society: Letters*, vol. 356, no. 1, pp. L11-L16, 2005. [CrossRef] [Google Scholar] [Publisher Link]

[11] E.M. Barboza Jr., and Jailson Souza de Alcaniz, "A Parametric Model for Dark Energy," *Physics Letters B*, vol. 666, no. 5, pp. 415-419, 2008. [CrossRef] [Google Scholar] [Publisher Link]

[12] Eric V. Linder, and Dragan Huterer, "How Many Dark Energy Parameters?," *Physical Review D*, vol. 72, no. 4, pp. 1-10, 2005. [CrossRef] [Google Scholar] [Publisher Link]

[13] M. Abdul-Karim et al., "DESI DR2 Results II: Measurements of Baryon Acoustic Oscillations and Cosmological Constraints," *Physical Review D*, vol. 112, no. 8, pp. 1-40, 2025. [CrossRef] [Google Scholar] [Publisher Link]

[14] Kushal Lodha et al., "Extended Dark Energy Analysis using DESI DR2 BAO Measurements," *Physical Review D*, vol. 112, no. 8, pp. 1-27, 2025. [CrossRef] [Google Scholar] [Publisher Link]

[15] George Efstathiou, "Evolving Dark Energy or Supernovae Systematics?," *Monthly Notices of the Royal Astronomical Society*, vol. 538, no. 2, pp. 875-882, 2025. [CrossRef] [Google Scholar] [Publisher Link]

[16] Deng Wang, and David Mota, "Did DESI DR2 Truly Reveal Dynamical Dark Energy?," *The European Physical Journal C*, vol. 85, no. 11, pp. 1-6, 2025. [CrossRef] [Google Scholar] [Publisher Link]

[17] Marina Cortês, and Andrew R. Liddle, "Interpreting DESI's Evidence for Evolving Dark Energy," *Journal of Cosmology and Astroparticle Physics*, vol. 2024, no. 12, pp. 1-10, 2024. [CrossRef] [Google Scholar] [Publisher Link]

[18] Marina Cortês, and Andrew R. Liddle, "On DESI's DR2 Exclusion of ΛCDM," *Monthly Notices of the Royal Astronomical Society: Letters*, vol. 544, no. 1, pp. L121-L125, 2025. [CrossRef] [Google Scholar] [Publisher Link]

[19] Alexander Vikman, "Can Dark Energy Evolve to the Phantom?," *Physical Review D*, vol. 71, no. 2, pp. 1-15, 2005. [CrossRef] [Google Scholar] [Publisher Link]

[20] Ruiqi Chen et al., "Quintessential Dark Energy Crossing the Phantom Divide," *arXiv preprint*, pp. 1-11, 2025. [CrossRef] [Google Scholar] [Publisher Link]

[21] Dimitrios Efstratiou, Evangelos Achilleas Paraskevas, and Leandros Perivolaropoulos, "Addressing the DESI DR2 Phantom-Crossing Anomaly and Enhanced H0 Tension with Reconstructed Scalar-Tensor Gravity," *Physical Review D*, vol. 113, no. 12, pp. 1-32, 2025. [CrossRef] [Google Scholar] [Publisher Link]

[22] Wenjuan Fang, Wayne Hu, and Antony Lewis, "Crossing the Phantom Divide with Parameterized Post-Friedmann Dark Energy," *Physical Review D*, vol. 78, no. 8, pp. 1-4, 2008. [CrossRef] [Google Scholar] [Publisher Link]

[23] Ryan E. Keeley, Arman Shafieloo, and William L. Matthewson, "Could We Be Fooled about Phantom Crossing?," *arXiv preprint*, pp. 1-6, 2025. [CrossRef] [Google Scholar] [Publisher Link]

[24] Xue Zhang, Yin-Hao Xu, and Yu Sang, "Reconstruction of Dark Energy using DESI DR2," *arXiv preprint*, pp. 1-11, 2025. [Google Scholar] [Publisher Link]

[25] Varun Sahni et al., "Statefinder—A New Geometrical Diagnostic of Dark Energy," *Journal of Experimental and Theoretical Physics Letters*, vol. 77, no. 5, pp. 201-206, 2003. [CrossRef] [Google Scholar] [Publisher Link]

[26] Varun Sahni, Arman Shafieloo, and Alexei A. Starobinsky, "Two New Diagnostics of Dark Energy," *Physical Review D*, vol. 78, no. 10, pp. 1-14, 2008. [CrossRef] [Google Scholar] [Publisher Link]

[27] Matt Visser, "Jerk, Snap and the Cosmological Equation of State," *Classical and Quantum Gravity*, vol. 21, no. 11, pp. 2603-2615, 2004. [CrossRef] [Google Scholar] [Publisher Link]

[28] Gabriel Rodrigues, Rayff de Souza, and Jailson Alcaniz, "Cosmography with DESI DR2 and SN Data," *arXiv preprint*, pp. 1-7, 2025. [CrossRef] [Google Scholar] [Publisher Link]

[29] Sai Swagat Mishra et al., "DESI DR2 Meets Cosmography: A Comparative Study of Padé, Chebyshev, and Taylor Expansions," *Monthly Notices of the Royal Astronomical Society*, vol. 546, no. 4, pp. 1-6, 2026. [CrossRef] [Google Scholar] [Publisher Link]

[30] Elisa Fazzari, William Giarè, and Eleonora Di Valentino, "Cosmographic Footprints of Dynamical Dark Energy," *arXiv preprint*, pp. 1-29, 2025. [CrossRef] [Google Scholar] [Publisher Link]

[31] Jincheng Wang, Hongwei Yu, and Puxun Wu, "Revisiting Cosmic Acceleration with DESI BAO," *The European Physical Journal C*, vol. 85, no. 8, pp. 1-9, 2025. [CrossRef] [Google Scholar] [Publisher Link]

[32] Dale J. Fixsen, "The Temperature of the Cosmic Microwave Background," *The Astrophysical Journal*, vol. 707, no. 2, pp. 916-920, 2009. [CrossRef] [Google Scholar] [Publisher Link]

[33] Robert R. Caldwell, Marc Kamionkowski, and Nevin N. Weinberg, "Phantom Energy: Dark Energy with $w < -1$ Causes a Cosmic Doomsday," *Physical Review Letters*, vol. 91, no. 7, pp. 1-4, 2003. [CrossRef] [Google Scholar] [Publisher Link]